JBC Papers in Press. Published on May 16, 2017 as Manuscript M117.788547
The latest version is at http://www.jbc.org/cgi/doi/10.1074/jbc.M117.788547

H_2S oxidation by nanodisc-embedded human sulfide quinone oxidoreductase

Aaron P. Landry, David P. Ballou and Ruma Banerjee*

Department of Biological Chemistry, University of Michigan Medical School, Ann Arbor, MI 48109

Running Title: SQR reaction mechanism

*Address correspondence to: Ruma Banerjee, 4220C MSRB III, 1150 W. Medical Center Dr., University of Michigan, Ann Arbor, MI 48109-0600, Tel: (734) 615-5238; E-mail: rbanerje@umich.edu

Buildup of hydrogen sulfide (H_2S), which functions as a signaling molecule but is toxic at high concentrations, is averted by its efficient oxidation by the mitochondrial sulfide oxidation pathway. The first step in this pathway is catalyzed by a flavoprotein, sulfide quinone oxidoreductase (SQR), which converts H_2S to a persulfide and transfers electrons to coenzyme Q via a flavin cofactor. All previous studies on human SQR have used detergent-solubilized protein. Here, we embedded human SQR in nanodiscs (*nd*SQR) and studied highly homogenous preparations by steady-state and rapid kinetics techniques. *nd*SQR exhibited higher catalytic rates in its membranous environment than in its solubilized state. Stopped-flow spectroscopic data revealed that transfer of the sulfane sulfur from an SQR-bound cysteine persulfide intermediate to a small-molecule acceptor is the rate-limiting step. The physiological acceptor of sulfane sulfur from SQR has been the subject of controversy; we report that the kinetic analysis of *nd*SQR is consistent with glutathione rather than sulfite being the predominant acceptor at physiologically relevant concentrations of the respective metabolites. The identity of the acceptor has an important bearing on how the sulfide oxidation pathway is organized. Our data are more consistent with the following reaction sequence for sulfide oxidation: $H_2S \rightarrow$ glutathione persulfide $\rightarrow$ sulfite $\rightarrow$ sulfate, than with a more convoluted route that would result if sulfite were the primary acceptor of sulfane sulfur. In summary, nanodisc-incorporated human SQR exhibits enhanced catalytic performance, and pre-steady state kinetic characterization of the complete SQR catalytic cycle indicates that GSH serves as the physiologically relevant sulfur acceptor.

Hydrogen sulfide (H_2S) is a signaling molecule that exerts varied effects in the cardiovascular, gastrointestinal and central nervous systems (1,2). In mammals, H_2S is produced enzymatically by cystathionine β-synthase and cystathionine γ-lyase in the transsulfuration pathway (3,4), as well as by 3-mercaptopyruvate sulfurtransferase (5,6). However, H_2S accumulation is toxic because it targets cytochrome *c* oxidase in the electron transport chain (7). Thus, low steady-state levels of H_2S are maintained primarily by the action of the mitochondrial sulfide oxidation pathway, which converts H_2S to thiosulfate and sulfate (8). The sulfide oxidation pathway is also postulated to facilitate H_2S-mediated signaling, via generation of reactive sulfur species (9).

The first step in the sulfide oxidation pathway is catalyzed by sulfide quinone oxidoreductase (SQR)[1]. SQR is anchored in the inner mitochondrial membrane and is a member of the flavin disulfide reductase family (10). It catalyzes a combination of a sulfur transfer reaction from H_2S to an acceptor via a cysteine persulfide (Cys-SSH) intermediate and an electron transfer reaction from H_2S to coenzyme Q (CoQ_{10}) via an $FADH_2$ intermediate (Fig. 1). The postulated reaction mechanism involves addition of H_2S to the active site disulfide formed between Cys-379 and Cys-201 to form Cys-SSH at Cys-379 with the release of the Cys-201 thiolate. The latter engages in an intensely absorbing charge transfer (CT) complex with FAD with an absorbance maximum

[1]SQR, sulfide quinone oxidoreductase; CoQ, coenzyme Q; Cys-SSH, cysteine persulfide; CT, charge transfer; GSSH, glutathione persulfide; PDO, persulfide dioxygenase; DHPC, 1,2-diheptanoyl-*sn*-glycero-3-phophocholine; MSP, MSP1E3D1 scaffold protein; POPC, 1-palmitoyl-2-oleoyl-*sn*-glycero-3-phosphocholine

at ~675 nm (9,11) Transfer of the sulfane sulfur from Cys-SSH to one of several acceptors completes the sulfur transfer reaction, yielding a small molecule persulfide and reduced $FADH_2$ (8,9,11,12). In the second half reaction, $FADH_2$ relays two electrons to oxidized CoQ_{10} to regenerate the resting enzyme. SQR exhibits remarkable substrate promiscuity, using a variety of small molecule acceptors *in vitro*, including cyanide, sulfite, sulfide, GSH, cysteine, and homocysteine (8,11,12) (Fig. 1A). The identity of the primary acceptor *in vivo* is unclear and in fact, is a matter of controversy. Due to the high reactivity of sulfite with the Cys-SSH intermediate in SQR, and the reported lack of GSH acceptor activity, it was initially concluded that sulfite functions as the primary sulfane sulfur acceptor (11). This view was soon challenged by the demonstration that GSH can indeed function as a sulfane sulfur acceptor at physiologically relevant concentrations of this thiol (12). Simulations using a range of sulfite concentrations from 0-100 μM predicted that sulfite would surpass the acceptor activity of GSH at concentrations >30 μM (12). While GSH concentrations are well determined and range from 1-10 mM depending on the cell type, the concentration of sulfite is poorly determined. A recent study, however, reported an intracellular sulfite concentration of 9.2 μM in rat liver (13). The authors used monobromobimane derivatization of tissue extract followed by HPLC analysis to estimate sulfite concentration. However, the identity of the compound(s) in the peak eluting with the same retention time as authentic sulfite was not validated by mass spectrometry or NMR spectroscopy. For reasons discussed later, it is highly probable that the sulfite concentration was overestimated in this study. The reactivity of sulfite (e.g., with some flavoproteins with K_D values in the nanomolar to low micromolar range (14)) is well known, and the presence of sulfite oxidase in compartments (e.g., the peroxisome), where sulfur assimilation does not occur, has been taken as evidence of its importance in removing toxic sulfite and maintaining low concentrations (15). The k_{cat}/K_M for the reaction of sulfite oxidase with sulfite is 2.4×10^6 $M^{-1}s^{-1}$ (16).

The issue of what constitutes the physiological acceptor of SQR is pertinent to understanding how the sulfide oxidation pathway is organized. If the product is thiosulfate (with sulfite as acceptor), then it must first be converted to GSSH, the only known substrate for persulfide dioxygenase (PDO, also known as ETHE1), which catalyzes the conversion of GSSH to sulfite and GSH (17,18). If on the other hand, the product is GSSH (with GSH as acceptor), then it can be directly utilized by PDO.

All prior studies on human SQR have used detergent-solubilized protein from membranes (9,11-13). Stopped-flow spectroscopic studies on solubilized protein were used to characterize the kinetics of the first detectable step, i.e. CT complex formation (9). Since SQR is a membrane protein, it is important that its catalytic properties and efficacy with sulfite versus GSH as the acceptor be assessed in a more native membrane-like environment. To this end, we have incorporated human SQR into nanodiscs (*nd*SQR), generating soluble, monodisperse, and stable protein in the absence of detergent. *nd*SQR exhibits enhanced activity compared to the previously studied solubilized protein. Stopped-flow spectroscopic characterization of *nd*SQR revealed enhanced sulfide binding and that sulfane sulfur transfer from Cys-SSH to either GSH or sulfite constitutes the rate-limiting step. In contrast, electrons are rapidly transferred from *nd*SQR-bound $FADH_2$ to CoQ. This study provides the kinetic framework for assessing the SQR reaction in the context of the mitochondrial sulfide oxidation pathway.

RESULTS

Incorporation of human SQR into nanodiscs-The purification procedure developed previously for human SQR involves extraction of the recombinant enzyme from *E. coli* membranes and solubilization using DHPC, a phospholipid detergent with short fatty acid chains (11,12). To transition the solubilized SQR into nanodiscs, we combined the enzyme with the MSP1E3D1 scaffold protein (MSP) (19,20) and the phospholipid POPC as described under Experimental Procedures. A molar ratio of 1:1:130 for SQR/MSP/POPC was used to incorporate one SQR dimer per nanodisc, containing 2 MSPs and ~125 POPC molecules per disc leaflet (21). Upon

purification by gel filtration, *nd*SQR eluted at a position consistent with the Stokes diameter of ~13 nm for MSP1E3D1 nanodiscs assembled with POPC (Fig. 2A, black trace) (19,20). This nanodisc peak overlapped with the 450 nm absorbance of the FAD cofactor in SQR (Fig. 2A, gray circles) and both MSP and SQR were detected in the elution peak by SDS-PAGE (Fig. 2B). The assembled *nd*SQR was further assessed by SEC-MALS, which yielded an estimated molecular mass of ~303 kDa and a polydispersity index of 1.007 ± 0.06, corresponding to a monodisperse population (Fig. 2C). The FAD spectrum of *nd*SQR was virtually identical to that of solubilized SQR, with absorbance maxima at 385 and 450 nm (Fig. 2D). The A_{450}:A_{280} ratio of ~10:1 obtained with detergent-solubilized SQR (11,12) was increased to ~13:1 with *nd*SQR due to the presence of MSP (Fig. 2D, *inset*).

Steady-state kinetic characterization of ndSQR with small-molecule acceptors-We characterized sulfide-driven reduction of CoQ_1 by *nd*SQR in the presence of various concentrations of sulfite, sulfide or GSH (Fig. 3). In comparison to solubilized SQR, *nd*SQR showed somewhat greater activity with all acceptors tested (Table 1). The catalytic efficiency (k_{cat}/K_M) of the *nd*SQR reaction with sulfite, GSH and sulfide was 25%, 45% and 100% greater, respectively, than that of solubilized SQR. We note that the K_M for GSH was previously overestimated (12) due to the contribution of a non-enzymatic, GSH-dependent CoQ_1 reduction activity (13), determined to be ~1.6 μmol CoQ_1 min^{-1} mM GSH^{-1} under our assay conditions. Correcting for this background yielded an ~3-fold lower value for K_M for GSH using solubilized SQR, which was identical to that obtained with *nd*SQR.

Kinetics of the sulfide-induced charge transfer complex formation in ndSQR—Addition of sulfide to SQR leads to the formation of an enzyme-bound Cys-SSH intermediate and a prominent CT band due to the interaction of the thiolate with FAD, and has a characteristic absorbance maximum at 675 nm (11,12). Stopped-flow spectroscopic analysis of CT complex development with *nd*SQR revealed identical spectral changes as seen with solubilized SQR, including increases in absorbance at 390 nm and 675 nm and a decrease in absorbance at 450 nm, with isosbestic points at 423 and 500 nm (Fig. 4A). The k_{on} rate for sulfide binding to *nd*SQR (4×10^6 $M^{-1}s^{-1}$) was 2-fold higher than observed with solubilized SQR (2×10^6 $M^{-1}s^{-1}$); the k_{off} rates were similar (48 ± 6 s^{-1} versus 46 ± 3 s^{-1}). Thus, the apparent K_D for sulfide binding to *nd*SQR (12 μM) is nearly 2-fold lower versus solubilized SQR (22 μM), indicating a higher binding affinity for sulfide when SQR is in its native membrane environment. Due to the presence of excess sulfide, the CT complex decayed slowly (~0.02 s^{-1}) with concomitant reduction of FAD (Fig. 4C) as seen previously with solubilized SQR (9).

Kinetics of GSH- and sulfite-dependent decay of the CT complex in ndSQR-The rate constant for the decay of the CT complex in the presence of either GSH or sulfite has not been previously evaluated. Double-mixing stopped-flow studies with *nd*SQR were employed to assess the kinetic competence of sulfane sulfur transfer from Cys-SSH to either GSH or sulfite as monitored by the decay of the CT complex, which was accompanied by reduction of FAD. For this, *nd*SQR was mixed with two equivalents of sulfide to form the CT complex, which was found to be stable for several seconds (Fig. 5A). After aging for ~35 ms, GSH was introduced via a third syringe, which led to a rapid decrease in 675 nm absorbance of the CT complex (Fig. 5A) as FAD became reduced (Fig. 5B). The k_{obs} for CT complex decay was linearly dependent on the concentration of GSH, yielding a k_{off} of 1.3 ± 0.2 s^{-1}, k_{on} of 3×10^2 M^{-1} s^{-1}, and an apparent K_D of 4 mM at 4 °C (Fig. 5C).

Rapid decay of the CT complex was also observed in the presence of sulfite (Fig. 6A) forming reduced FAD (Fig. 6B). The k_{obs} for CT complex decay with sulfite was dependent on its concentration, yielding a k_{off} of 6.7 ± 0.8 s^{-1}, k_{on} of 3.9×10^5 M^{-1} s^{-1}, and an apparent K_D of 17 μM at 4 °C (Fig. 6C). The k_{obs} values for the decay of the CT complex in the presence of 50 mM GSH or 100 μM sulfite (16 ± 1 s^{-1} and 46 ± 3 s^{-1} at 4 °C, respectively) are similar to k_{cat} values obtained in the steady-state assay at the same substrate concentrations and temperature (13 ± 2 s^{-1} for GSH and 36 ± 2 s^{-1} for sulfite). This suggests that transfer of the sulfane sulfur from the active site Cys-SSH to the acceptor is the primary rate-determining step in the SQR reaction cycle.

Kinetic analysis of ndSQR-mediated CoQ_1 reduction-Sulfane sulfur transfer from Cys-SSH to the acceptor drives the reduction of FAD to

$FADH_2$, which in turn reduces the native quinone substrate, CoQ_{10}. The rate of quinone reduction by *nd*SQR was determined under steady-state conditions by varying the concentration of the water-soluble analog, CoQ_1, at saturating concentrations of sulfide and sulfite. From this analysis, a value of 5 ± 0.2 μM was obtained for the K_M for CoQ_1 for *nd*SQR (Fig. 7). By comparison, an ~5-fold higher K_M value for CoQ_1 (24 ± 3 μM) was obtained with solubilized SQR, which was consistent with a previous report (11).

The kinetic competence of the CoQ_1 reduction half-reaction by *nd*SQR was investigated by stopped-flow studies. Since full reduction of *nd*SQR requires an excess of sulfide, its use would lead to enzyme turnover in the presence of CoQ_1 (Fig. 1). Therefore, *nd*SQR was pre-reduced by photoreduction with 5-deazaflavin. Rapid mixing of CoQ_1 with reduced *nd*SQR led to rapid flavin oxidation (Fig. 8A). The dependence of the k_{obs} rates for *nd*SQR-bound $FADH_2$ oxidation was hyperbolic versus CoQ_1 concentration yielding an apparent K_D of 20 μM (Fig. 8B). The k_{obs} rate approached a maximum of ~250 s^{-1} at CoQ_1 concentrations ≥50 μM. It is likely that CoQ_{10} reduction by SQR *in vivo* could proceed at a similar or even higher rate given that the hepatic concentration of CoQ_{10} is ~100 μM (22).

DISCUSSION

As a membrane protein, the study of human SQR has been limited by its insolubility and relative instability in aqueous solution. Furthermore, the use of detergent-solubilized protein could affect conformational dynamics and/or substrate access to SQR. Nanodiscs have proven to be powerful tools for studying membrane proteins, and in several cases have led to improved kinetic behavior via effects ranging from subtle conformational shifts to changes in oligomerization states (23). In this study, we have prepared SQR incorporated into nanodiscs to compare its catalytic performance with detergent-solubilized protein, characterized the full catalytic cycle by stopped-flow spectroscopy, and obtained the relevant kinetic parameters in a lipid bilayer environment to address the controversy regarding the physiological sulfane sulfur acceptor.

The steady-state kinetic parameters for *nd*SQR reveals improved catalytic performance (k_{cat}/K_M) over that of detergent-solubilized SQR, particularly with sulfide (~100%) and GSH (45%) (Table 1). Notably, the K_M for GSH (8 ± 1 mM) is significantly lower than previously reported (22 ± 3 mM) (12), which can be attributed to correction of the background nonenzymatic rate of CoQ reduction by GSH. This background rate was previously postulated to be an SQR-mediated GSH:CoQ_1 oxidoreductase activity (13) but was found in our studies to occur in the absence of SQR.

Our previous study of the pre-steady state kinetics of solubilized SQR was limited to analysis of the first step in the reaction, i.e., formation of the CT complex in the presence of sulfite or sulfide (9). CT complex formation with sulfide was shown to be rapid (3.4×10^5 M^{-1} s^{-1} at pH 7.4 and 4 °C) and kinetically competent (9). In contrast, addition of sulfite to SQR to form sulfocysteine (Cys-S-SO_3^{2-}), exhibited an ~3000-fold lower rate constant under the same conditions (1×10^2 M^{-1} s^{-1}). This observation ruled out an alternative mechanism in which sulfite adds first and the resulting sulfocysteine intermediate is resolved by sulfide to form thiosulfate. In this study, we have determined a bimolecular rate constant for sulfide addition to *nd*SQR at 4 °C of 4×10^6 M^{-1} s^{-1}, which is greater than for the solubilized protein (Fig. 4). H_2S is slightly hydrophobic and its partition coefficient is 2 ± 0.6 (at 25 °C) in a dilauroyl phosphatidylcholine liposome/water mixture (24). Hence, the higher reaction rate of H_2S with *nd*SQR than with the solubilized protein could be explained by its ability to concentrate in membranes leading to an increase in its local concentration in nanodiscs.

We have determined for the first time, the rates of the individual reactions beyond the CT complex formation step (Fig. 1B). The rates of transfer of the sulfane sulfur group from *nd*SQR to small molecule acceptors were determined in double mixing experiments by stopped-flow spectroscopy (Figs. 5,6). The k_{obs} values for sulfane sulfur transfer to GSH or to sulfite were similar to the steady state k_{cat} values under the same experimental conditions. Hence, transfer of the sulfane sulfur from cysteine persulfide to GSH (or sulfite), with concomitant reduction of FAD, is the rate-limiting step in SQR catalysis. The k_{off} for

sulfite (6.7 ± 0.8 $s^{-}1$) is 5-fold greater than for GSH (1.3 ± 0.2 s^{-1}), which is consistent with their difference in size and the greater potential for binding interactions between GSH and the active site residues of SQR. Although the k_{on} for sulfite (3.9 × 10^5 M^{-1} s^{-1}) is 1,300–fold greater than for GSH (3× 10^2 M^{-1} s^{-1}), the difference in their k_{cat} values (under V_{max} conditions) is only 5-fold (Table 1). This discrepancy between the 1,300-fold greater association rate constant for sulfite versus GSH but only a 5-fold greater k_{cat}, suggests that one or more of the steps following acceptor binding, i.e., FAD reduction, re-formation of the disulfide and transfer of the sulfane sulfur, occurs more efficiently with GSH as acceptor than with sulfite.

The final step in the reaction cycle, reduction of CoQ_1 by $FADH_2$, is very rapid (Fig. 8). The K_M for CoQ_1 is 5-fold lower for SQR incorporated into nanodiscs than for solubilized SQR (Fig. 7). The quinone pool resides in the mitochondrial inner membrane, and its interaction with SQR requires entry into the quinone binding site at the protein-membrane interface, as seen in the structure of *Acidithiobacillus ferrooxidans* SQR (25). The lower K_M for CoQ_1 observed with *nd*SQR might be due not only to the enhanced efficiency of CoQ_1 entry into the quinone binding site, but also due to sequestering of CoQ_1 in nanodiscs, thus increasing its local concentration. The natural substrate for SQR is CoQ_{10}, which is more hydrophobic and because it could partition even more favorably into the membrane, could potentially react even more rapidly than CoQ_1 (~250 s^{-1} at ≥50 μM CoQ_1). Reduction of CoQ integrates H_2S oxidation with the electron transport chain by providing reduced quinone to complex III (26).

With the kinetic parameters obtained with *nd*SQR, the question of its physiological sulfane sulfur acceptor can now be re-evaluated. Although GSH exhibits a lower catalytic efficiency (k_{cat}/K_M = 1.6 × 10^4 $M^{-1}s^{-1}$) than sulfite (2.5 × 10^6 $M^{-1}s^{-1}$), it is far more abundant in the cell. The K_M value for GSH (8 ± 1 mM) is within the range of its intracellular concentration. In contrast, the K_M for sulfite (260 ± 30 μM) is significantly higher than the intracellular sulfite concentration, which is in fact, not well known. Other than a few reports of sulfite concentration in human serum and plasma, in which it is very low (<20 nM for free sulfite and 0.47-4.6 μM for total (free + bound) sulfite) (27,28), a recent report of intracellular sulfite estimated it to be 9.2 μM in rat liver and even higher in heart (13). To compensate for the then undetermined intracellular concentration of sulfite, we had previously used kinetic simulations over a sulfite concentration range of 0-100 μM. The kinetic simulations predicted that GSH (even with the higher $K_{M(GSH)}$ value of 22 ± 3 mM used in that study) is the dominant acceptor at <30 μM sulfite concentrations (12). Using the corrected K_M for GSH and the k_{cat}/K_M, values for *nd*SQR determined in this study (Table 1), we can estimate turnover number of 112 s^{-1} at 7 mM GSH (liver concentration (29,30)) versus 23 s^{-1} at 9.2 μM sulfite. Based on these estimates derived from steady-state kinetic parameters alone, GSH is favored ~5:1 over sulfite as an acceptor. However, as discussed below, it is likely that the preference for GSH is much greater than 5-fold under cellular conditions.

The prevalence of substrate promiscuity in enzyme-catalyzed reactions (31) including those involved in H_2S biogenesis (32), is well known. Typically, promiscuity arises from the ability of structurally related substrates to compete for the same binding site. In the case of SQR, it would be remarkable if an active site that had evolved to bind sulfite would coincidentally also bind the tripeptide substrate, i.e. GSH, as has been suggested (11,13). Instead, we conclude that an active site that can accommodate GSH can in principle, bind smaller substrates (e.g., homocysteine, cysteine and sulfite, each of which serves as alternative acceptors (12)) and that these side reactions are averted in cells by the high K_M values of these alternative acceptors versus their intracellular concentrations. In this context, it is critically important to have a rigorously determined value for the intracellular sulfite concentration.

The reactivity of sulfite, a six-electron oxidized product of H_2S, with aldehydes and DNA is well known, and its toxicity (33) has been exploited in the food industry for use as a preservative. In fact, the toxicity and anti-nutritional effects of sulfite (via depletion of thiamin and folic acid) (34) has led to an FDA ban on its use as a preservative in certain foods. It is very likely that the intracellular concentration of liver sulfite is kept low due to the high abundance and activity of sulfite oxidase in

this tissue (35). The 9.2 μM value is likely to be an overestimate, possibly resulting from the lack of analytical evaluation beyond the co-elution of an unknown peak from tissue lysates with authentic sulfite standard (13). Sulfur metabolite analysis from tissue extracts is routinely performed in our laboratory for detecting metabolites in the 0.01-10 mM concentration range (29,30,36) and the identity of all new metabolites is validated by mass spectrometric analysis following HPLC separation (e.g., (3)). Based on our studies, we conclude that intracellular sulfite concentration in murine liver is too low to be reliably determined by HPLC-based analysis (Vitvitsky and Banerjee, unpublished results). It is likely that other compounds in tissue lysates, co-eluting with sulfite, contributed to its overestimation by HPLC analysis in the recent study (13).

The identity of the sulfane sulfur acceptor has important implications for how the sulfide oxidation pathway is organized. While GSSH can be utilized directly by PDO (Fig. 9A), thiosulfate formed from sulfite cannot. Instead, thiosulfate must first undergo a second sulfur transfer to generate GSSH, before it can be re-oxidized to sulfite by PDO (Fig. 9B). Rhodanese is a mitochondrial sulfurtransferase that catalyzes the reversible transfer of sulfane sulfur between GSSH and sulfite ($GSSH + SO_3^{2-} \Leftrightarrow GSH + S_2O_3^{2-}$). In principle, it could serve as the sulfurtransferase that generates GSSH from thiosulfate. However, human rhodanese and its common polymorphic variants exhibit an ~217,000-fold preference for sulfur transfer in the direction of $GSSH \rightarrow S_2O_3^{2-}$ with a k_{cat} of 389 s^{-1} at pH 7.4 and 37 ºC (12,37). The only other known sulfurtransferase that can support the conversion of thiosulfate to GSSH (i.e., $GSH + S_2O_3^{2-} \Leftrightarrow GSSH + SO_3^{2-}$) is TSTD1, which exhibits a K_M for thiosulfate of 14 mM and a low k_{cat} (2.7 s^{-1} at optimum pH of 9 and 37 ºC). Its involvement in the sulfide oxidation pathway would necessitate the intercompartmental crossing of the highly reactive GSSH intermediate from the cytoplasm to the mitochondrion (Fig. 9B). This alternative pathway was described as "convoluted" even by its proponents (11).

The clinical data on sulfur metabolite accumulation in PDO or rhodanese dysfunction, or thiosulfate catabolism, can be interpreted to support either organizational scheme for H_2S oxidation (11-13). In the absence of metabolic flux analysis combined with gene knockdown studies, use of these data to distinguish between pathways should be treated with caution.

In summary, we report the enhanced catalytic performance of human SQR incorporated in nanodiscs and present a rapid pre-steady state kinetic characterization of the complete catalytic cycle. The proposal that the SQR active site evolved to accommodate sulfite, but accidentally allows a significantly larger and much more abundant molecule, i.e. GSH, to effectively compete, appears to be improbable. Our kinetic data on *nd*SQR, and the potential to directly funnel labile sulfur from SQR to PDO via GSH, support our conclusion that GSH serves as the physiologically relevant sulfur acceptor. The crystal structure of human SQR will allow this question to be addressed unequivocally.

EXPERIMENTAL PROCEDURES

Materials—The following reagents were purchased from Sigma-Aldrich: Amberlite XAD-2 resin, CoQ_1, GSH, sodium sulfide nonahydrate, sodium sulfite, and sodium cholate hydrate. The phospholipids, DHPC and POPC, were purchased from Anatrace Lipids (Maumee, OH). The photocatalyst 5-deazaflavin was a generous gift from Dr. Bruce Palfey (University of Michigan).

Incorporation of human SQR into nanodiscs—Human SQR was purified as reported previously (12). The membrane scaffold protein MSP1E3D1 (MSP) was expressed in *E. coli* BL21(DE3) cells using the $pET28b^+$ expression vector (plasmid # 20066, deposited to Addgene by Dr. Steven Sligar, University of Illinois at Urbana-Champaign) and purified as reported previously (19,38).

SQR was incorporated into nanodiscs by combining POPC, MSP, and SQR in a molar ratio of 130:1:1 in nanodisc buffer (20 mM Tris, pH 7.4, containing 150 mM NaCl and 0.5 mM EDTA) with 25 mM sodium cholate. The mixture was incubated on ice for 1 h. Nanodisc assembly was induced by the removal of cholate by adsorption on Amberlite XAD-2 resin. The resin was pre-equilibrated with nanodisc buffer and incubated

overnight with the assembly mixture at 4 °C with gentle agitation. The assembled nanodiscs were separated from the XAD-2 resin by filtration, and subsequently purified by gel filtration using a 25 ml Superdex 200 column (GE Healthcare) equilibrated with nanodisc buffer. The size of the assembled discs was estimated by comparison with gel filtration standards (Bio-Rad) with known Stokes diameters. The purity of *nd*SQR was evaluated on a 15% SDS-polyacrylamide gel. The estimated molecular weight and polydispersity index of purified *nd*SQR was estimated by size exclusion chromatography coupled with multi-angle light scattering (SEC-MALS, Wyatt Technology).

Spectral analysis of ndSQR—The electronic absorption spectra of *nd*SQR were recorded in 100 mM potassium phosphate buffer, pH 7.4. The same buffer containing DHPC (0.03%) was used for the detergent-solubilized enzyme. The concentrations of *nd*SQR and detergent-solubilized SQR were estimated using an extinction coefficient at 450 nm of 11,500 M^{-1} cm^{-1} for the FAD cofactor (11).

SQR activity assays—SQR activity was assessed at 25 °C by monitoring the reduction of CoQ_1 at 278 nm ($\Delta\varepsilon_{ox\text{-}red}$ = 12,000 M^{-1} cm^{-1}) as described previously (11,12). Stock solutions of CoQ_1 were prepared aerobically in 10 mM potassium phosphate, pH 6.8, containing 10% DHPC. For assays with GSH as the acceptor, the reaction rates were corrected for trace amounts CoQ_1 reduction by GSH as previously reported (13). The kinetic parameters K_M and V_{max} were obtained by fitting the data sets to the Michaelis-Menten equation.

Stopped-flow spectroscopy—All aerobic rapid-mixing spectroscopic experiments were carried out at 4 °C on an SF-DX2 double mixing stopped-flow system from Hi-Tech Scientific, equipped with a photodiode array detector (300-700 nm range). The sulfide concentration dependence of the k_{obs} for CT complex formation was monitored as described previously (9). Spectra and k_{obs} for the disappearance of the sulfide-induced CT complex in *nd*SQR in the presence of GSH or sulfite were obtained in double mixing experiments. For this, *nd*SQR (40 μM) in 100 mM potassium phosphate buffer, pH 7.4, was mixed with sulfide (80 μM) and the solution was allowed to age for ~35 ms before mixing it with varying concentrations of GSH or sulfite in the same buffer. The reported concentrations are before mixing and each mixing resulted in a 1:1 dilution (v/v). Sulfite concentrations were kept to <100 μM or below to minimize a competitive sulfite-induced CT complex formation previously observed in solubilized SQR (9). The kinetic traces at selected wavelengths were fitted using the KinetAsyst software.

Stopped-flow studies on the *nd*SQR-mediated reduction of CoQ_1 were carried out at 8 °C on an Applied Photophysics stopped-flow system housed in an anaerobic chamber and equipped with a photodiode array detector (300-700 nm range). The reduced form of *nd*SQR (20 μM) was generated under anaerobic conditions by mixing 20 μM *nd*SQR in 100 mM potassium phosphate buffer, pH 7.4, with 15 mM EDTA and 2 μM 5-deazaflavin as a photocatalyst. The mixture was purged with N_2 gas for 30 min in the dark, followed by exposure to high-intensity white light for 30 min on ice. Reduced *nd*SQR was then mixed with various concentrations of CoQ_1 (0 to 80 μM) in the stopped-flow spectrophotometer. The kinetic traces at selected wavelengths were fitted using Pro-Data SX software.

Acknowledgements
This work was supported in part by the National Institutes of Health (GM112455 to R.B and F32GM122357 to A.P.L). The authors thank Dr. Greg Campanello for assistance with the SEC-MALS analysis and Dr. Pramod Yadav for help with the initial experiments on solubilized SQR.

Author Disclosure Statement
No competing financial interest exists.

Author contributions

A. P. L. designed and performed the experiments, D.P.B helped with some of the stopped-flow experiments and with data analysis. R.B. helped conceive the experiments, analyzed the data and co-wrote the manuscript with A. P. L. All authors approved the final version of the manuscript.

REFERENCES

1. Kimura, H. (2010) Hydrogen sulfide: from brain to gut. *Antioxid. Redox Signal.* **12**, 1111-1123
2. Kabil, O., and Banerjee, R. (2010) The redox biochemistry of hydrogen sulfide. *J. Biol. Chem.* **285**, 21903-21907
3. Chiku, T., Padovani, D., Zhu, W., Singh, S., Vitvitsky, V., and Banerjee, R. (2009) H_2S biogenesis by cystathionine gamma-lyase leads to the novel sulfur metabolites, lanthionine and homolanthionine, and is responsive to the grade of hyperhomocysteinemia. *J. Biol. Chem.* **284**, 11601-11612
4. Singh, S., Padovani, D., Leslie, R. A., Chiku, T., and Banerjee, R. (2009) Relative contributions of cystathionine beta-synthase and gamma-cystathionase to H_2S biogenesis via alternative trans-sulfuration reactions. *J. Biol. Chem.* **284**, 22457-22466
5. Shibuya, N., Tanaka, M., Yoshida, M., Ogasawara, Y., Togawa, T., Ishii, K., and Kimura, H. (2009) 3-Mercaptopyruvate sulfurtransferase produces hydrogen sulfide and bound sulfane sulfur in the brain. *Antioxid. Redox Signal.* **11**, 703-714
6. Yadav, P. K., Yamada, K., Chiku, T., Koutmos, M., and Banerjee, R. (2013) Structure and kinetic analysis of H_2S production by human mercaptopyruvate sulfurtransferase. *J. Biol. Chem.* **288**, 20002-20013
7. Nicholls, P., and Kim, J. K. (1982) Sulphide as an inhibitor and electron donor for the cytochrome c oxidase system. *Can. J. Biochem.* **60**, 613-623
8. Hildebrandt, T. M., and Grieshaber, M. K. (2008) Three enzymatic activities catalyze the oxidation of sulfide to thiosulfate in mammalian and invertebrate mitochondria. *FEBS J.* **275**, 3352-3361
9. Mishanina, T. V., Yadav, P. K., Ballou, D. P., and Banerjee, R. (2015) Transient Kinetic Analysis of Hydrogen Sulfide Oxidation Catalyzed by Human Sulfide Quinone Oxidoreductase. *J. Biol. Chem.* **290**, 25072-25080
10. Argyrou, A., and Blanchard, J. S. (2004) Flavoprotein disulfide reductases: advances in chemistry and function. *Prog. Nucleic Acid Res. Mol. Biol.* **78**, 89-142
11. Jackson, M. R., Melideo, S. L., and Jorns, M. S. (2012) Human sulfide:quinone oxidoreductase catalyzes the first step in hydrogen sulfide metabolism and produces a sulfane sulfur metabolite. *Biochemistry* **51**, 6804-6815
12. Libiad, M., Yadav, P. K., Vitvitsky, V., Martinov, M., and Banerjee, R. (2014) Organization of the human mitochondrial H_2S oxidation pathway. *J. Biol. Chem.* **289**, 30901-30910
13. Augustyn, K. D., Jackson, M. R., and Jorns, M. S. (2017) Use of Tissue Metabolite Analysis and Enzyme Kinetics To Discriminate between Alternate Pathways for Hydrogen Sulfide Metabolism. *Biochemistry* **56**, 986-996
14. Massey, V., Muller, F., Feldberg, R., Schuman, M., Sullivan, P. A., Howell, L. G., Mayhew, S. G., Matthews, R. G., and Foust, G. P. (1969) The reactivity of flavoproteins with sulfite. Possible relevance to the problem of oxygen reactivity. *J. Biol. Chem.* **244**, 3999-4006
15. Nowak, K., Luniak, N., Witt, C., Wustefeld, Y., Wachter, A., Mendel, R. R., and Hansch, R. (2004) Peroxisomal localization of sulfite oxidase separates it from chloroplast-based sulfur assimilation. *Plant Cell Physiol.* **45**, 1889-1894
16. Johnson-Winters, K., Nordstrom, A. R., Emesh, S., Astashkin, A. V., Rajapakshe, A., Berry, R. E., Tollin, G., and Enemark, J. H. (2010) Effects of interdomain tether length and flexibility on the kinetics of intramolecular electron transfer in human sulfite oxidase. *Biochemistry* **49**, 1290-1296
17. Tiranti, V., Viscomi, C., Hildebrandt, T., Di Meo, I., Mineri, R., Tiveron, C., Levitt, M. D., Prelle, A., Fagiolari, G., Rimoldi, M., and Zeviani, M. (2009) Loss of ETHE1, a mitochondrial dioxygenase, causes fatal sulfide toxicity in ethylmalonic encephalopathy. *Nat. Med.* **15**, 200-205
18. Kabil, O., and Banerjee, R. (2012) Characterization of Patient Mutations in Human Persulfide Dioxygenase (ETHE1) Involved in H_2S Catabolism. *J. Biol. Chem.* **287**, 44561-44567

19. Denisov, I. G., Grinkova, Y. V., Lazarides, A. A., and Sligar, S. G. (2004) Directed self-assembly of monodisperse phospholipid bilayer Nanodiscs with controlled size. *J. Am. Chem. Soc.* **126**, 3477-3487
20. Denisov, I. G., McLean, M. A., Shaw, A. W., Grinkova, Y. V., and Sligar, S. G. (2005) Thermotropic phase transition in soluble nanoscale lipid bilayers. *J. Phys. Chem. B* **109**, 15580-15588
21. Bayburt, T. H., Grinkova, Y. V., and Sligar, S. G. (2002) Self-assembly of discoidal phospholipid bilayer nanoparticles with membrane scaffold proteins. *Nano Letters* **2**, 853-856
22. Beyer, R. E., Burnett, B. A., Cartwright, K. J., Edington, D. W., Falzon, M. J., Kreitman, K. R., Kuhn, T. W., Ramp, B. J., Rhee, S. Y., Rosenwasser, M. J., and et al. (1985) Tissue coenzyme Q (ubiquinone) and protein concentrations over the life span of the laboratory rat. *Mech. Ageing Dev.* **32**, 267-281
23. Bayburt, T. H., and Sligar, S. G. (2010) Membrane protein assembly into Nanodiscs. *FEBS Lett* **584**, 1721-1727
24. Cuevasanta, E., Denicola, A., Alvarez, B., and Moller, M. N. (2012) Solubility and permeation of hydrogen sulfide in lipid membranes. *PloS One* **7**, e34562
25. Cherney, M. M., Zhang, Y., Solomonson, M., Weiner, J. H., and James, M. N. (2010) Crystal structure of sulfide:quinone oxidoreductase from Acidithiobacillus ferrooxidans: insights into sulfidotrophic respiration and detoxification. *J. Mol. Biol.* **398**, 292-305
26. Goubern, M., Andriamihaja, M., Nubel, T., Blachier, F., and Bouillaud, F. (2007) Sulfide, the first inorganic substrate for human cells. *FASEB J.* **21**, 1699-1706
27. Togawa, T., Ogawa, M., Nawata, M., Ogasawara, Y., Kawanabe, K., and Tanabe, S. (1992) High performance liquid chromatographic determination of bound sulfide and sulfite and thiosulfate at their low levels in human serum by pre-column fluorescence derivatization with monobromobimane. *Chem. Pharm. Bull. (Tokyo)* **40**, 3000-3004
28. Ji, A. J., Savon, S. R., and Jacobsen, D. W. (1995) Determination of total serum sulfite by HPLC with fluorescence detection. *Clin. Chem.* **41**, 897-903
29. Vitvitsky, V., Dayal, S., Stabler, S., Zhou, Y., Wang, H., Lentz, S. R., and Banerjee, R. (2004) Perturbations in homocysteine-linked redox homeostasis in a murine model for hyperhomocysteinemia. *Am. J. Physiol. Regu.l Integr. Comp. Physiol* .**287**, R39-46
30. Vitvitsky, V., Martinov, M., Ataullakhanov, F., Miller, R. A., and Banerjee, R. (2013) Sulfur-based redox alterations in long-lived Snell dwarf mice. *Mech. Ageing Dev.* **134**, 321-330
31. Khersonsky, O., and Tawfik, D. S. (2010) Enzyme promiscuity: a mechanistic and evolutionary perspective. *Annu. Rev. Biochem.* **79**, 471-505
32. Banerjee, R. (2017) Catalytic promiscuity and heme-dependent redox regulation of H2S synthesis. *Curr. Opin. Chem. Biol.* **37**, 115-121
33. Gunnison, A. F. (1981) Sulphite toxicity: a critical review of in vitro and in vivo data. *Food Cosmet. Toxicol.* **19**, 667-682
34. Stammati, A., Zanetti, C., Pizzoferrato, L., Quattrucci, E., and Tranquilli, G. B. (1992) In vitro model for the evaluation of toxicity and antinutritional effects of sulphites. *Food. Addit. Contam.* **9**, 551-560
35. Woo, W. H., Yang, H., Wong, K. P., and Halliwell, B. (2003) Sulphite oxidase gene expression in human brain and in other human and rat tissues. *Biochem. Biophys. Res. Commun.* **305**, 619-623
36. Vitvitsky, V. M., Garg, S. K., Keep, R. F., Albin, R. L., and Banerjee, R. (2012) Na(+) and K(+) ion imbalances in Alzheimer's disease. *Biochim. Biophys. Acta* **1822**, 1671-1681
37. Libiad, M., Sriraman, A., and Banerjee, R. (2015) Polymorphic Variants of Human Rhodanese Exhibit Differences in Thermal Stability and Sulfur Transfer Kinetics. *J. Biol. Chem.* **290**, 23579-23588
38. Boldog, T., Li, M., and Hazelbauer, G. L. (2007) Using Nanodiscs to create water-soluble transmembrane chemoreceptors inserted in lipid bilayers. *Methods Enzymol.* **423**, 317-335

TABLE 1

Kinetic parameters for H_2S oxidation by *nd*SQR versus solubilized SQR

Acceptor	SQR	K_M	V_{max}	k_{cat}	k_{cat}/K_M
		mM	μmol/min/mg	s^{-1}	$M^{-1} s^{-1}$
sulfite	in nanodiscs	0.26 ± 0.03	830 ± 34	650 ± 27	2.5×10^6
	solubilized	0.19 ± 0.01	488 ± 8	382 ± 6	2.0×10^6
sulfide	in nanodiscs	0.23 ± 0.02	107 ± 2	84 ± 2	3.7×10^5
	solubilized	0.35 ± 0.05	79 ± 4	62 ± 3	1.8×10^5
GSH	in nanodiscs	8 ± 1	164 ± 6	128 ± 5	1.6×10^4
	solubilized	8 ± 1	113 ± 6	89 ± 5	1.1×10^4

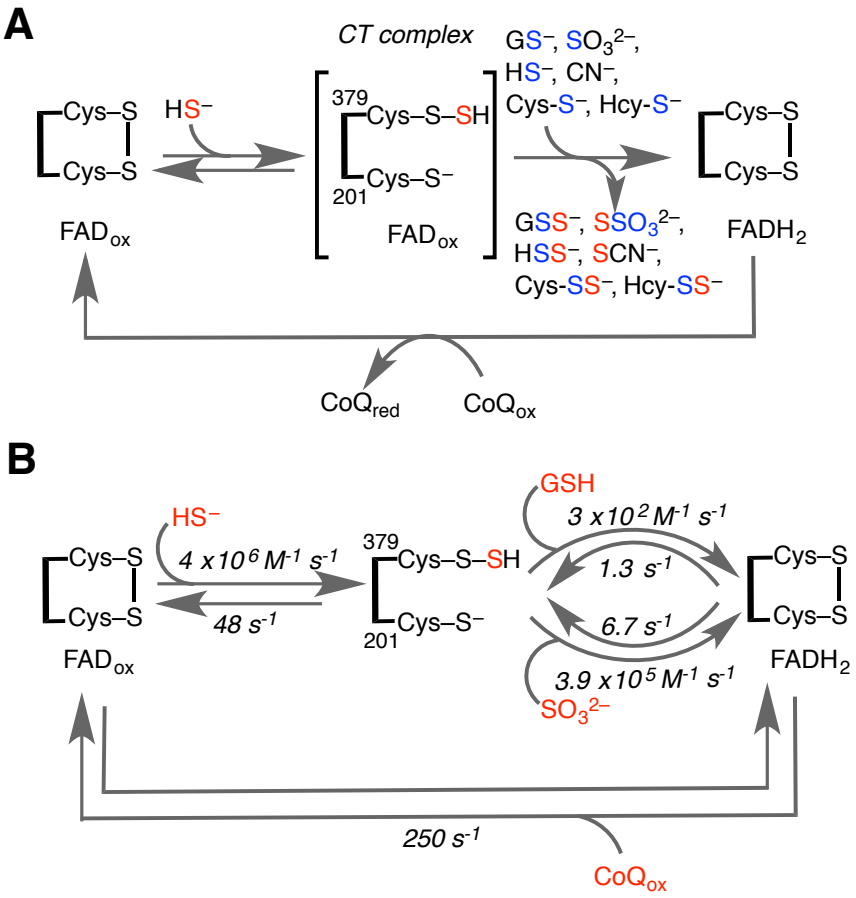

Figure 1. Minimal reaction mechanism of SQR. *A*, Reaction of sulfide (red) with the resting form of SQR leads to the formation of a Cys-SSH intermediate and the CT complex. A variety of acceptors (glutathione, sulfite, sulfide, cyanide, cysteine (Cys-S$^-$) and homocysteine (Hcy-S$^-$), shown in blue), can accept the sulfane sulfur as two electrons are transferred to FAD to give $FADH_2$. Oxidation of the latter by CoQ regenerates the resting enzyme. *B*, The rate constants for the individual steps for *nd*SQR determined in this study, are shown.

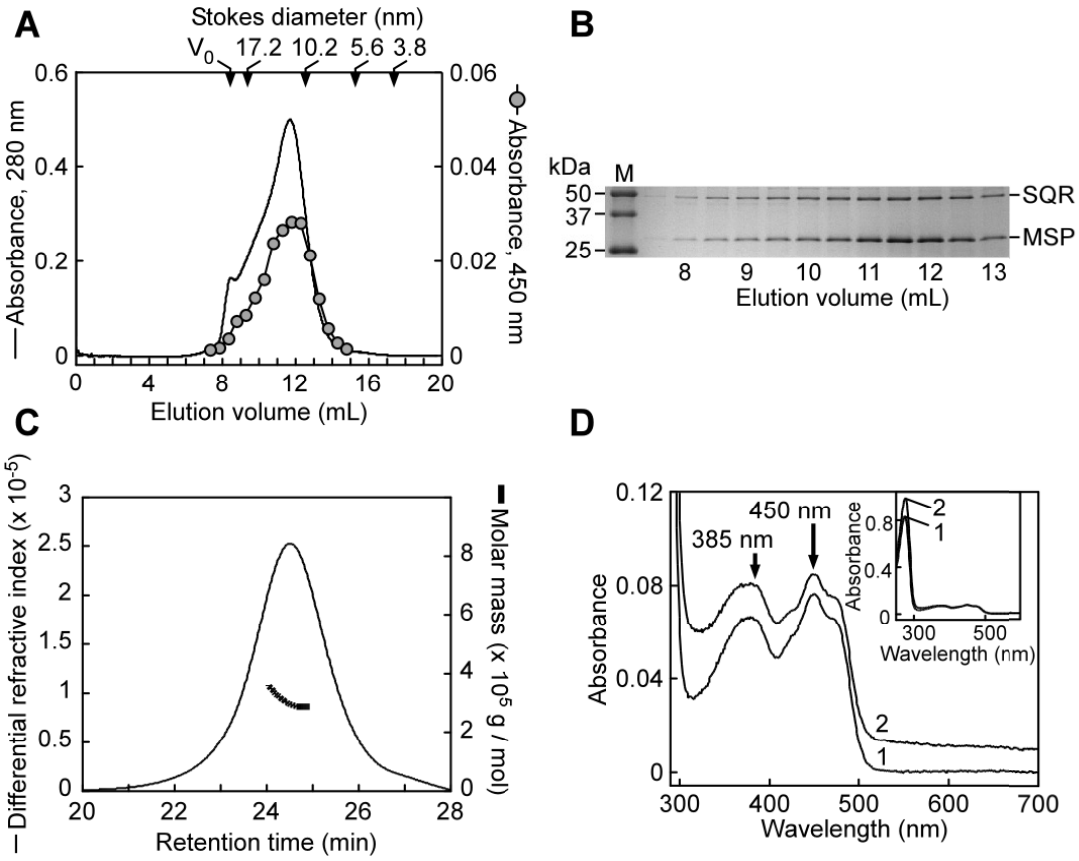

Figure 2. Incorporation of human SQR into nanodiscs. *A*, Elution profile of *nd*SQR in nanodisc buffer. The elution was monitored at 280 nm (solid black line) and individual fractions were measured for FAD absorbance at 450 nm (gray circles). V_0 denotes the void volume. The denoted Stokes diameters are derived from gel filtration standards in nanodisc buffer and represent thyroglobulin (670 kDa, D_S = 17.2 nm), γ-globulin (158 kDa, D_S = 10.2 nm), ovalbumin (44 kDa, D_S = 5.6 nm), and myoglobin (17 kDa, D_S = 3.8 nm), respectively. *B*, SDS-PAGE analysis of eluted gel filtration fractions of *nd*SQR, containing SQR (47 kDa) and the MSP (32.6 kDa). Molecular weight markers are shown in lane M. *C*, SEC-MALS elution profile of purified *nd*SQR in 50 mM HEPES, pH 7.5, containing 150 mM KCl, 2 mM $MgCl_2$ and 2 mM DTT. The refractive index (thin trace) and molar mass (thick trace) are plotted versus retention time. *D*, UV-visible absorbance spectra of detergent solubilized SQR (spectrum 1, 6.7 μM in nanodisc buffer containing 0.03% DHPC) compared to *nd*SQR (spectrum 2, 6.7 μM in nanodisc buffer, offset for clarity).

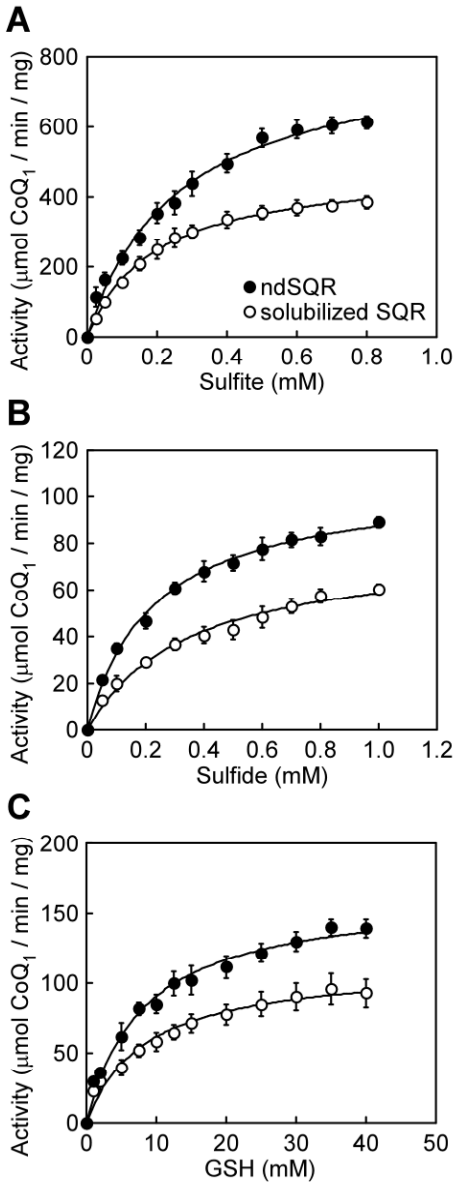

Figure 3. Steady-state kinetic characterization of H_2S oxidation by *nd*SQR in nanodiscs with varying concentrations of small molecule acceptors. The rates of sulfide-driven CoQ_1 reduction were assayed with *nd*SQR (closed circles) versus detergent solubilized enzyme (open circles). The reactions included 0–0.8 mM sulfite (*A*), 0–1 mM sulfide (*B*), or 0–40 mM GSH (*C*) in 100 mM potassium phosphate buffer, pH 7.4, containing 60 µM CoQ_1, 0.06 mg mL^{-1} BSA, 1 nM SQR, and 150 µM sulfide (except when sulfide was used as an acceptor in the reaction) at 25 °C. Assays with detergent solubilized SQR were conducted in the presence of 0.03% DHPC. The data represent the mean ± standard deviation for three independent experiments in which each acceptor concentration was assayed in duplicate.

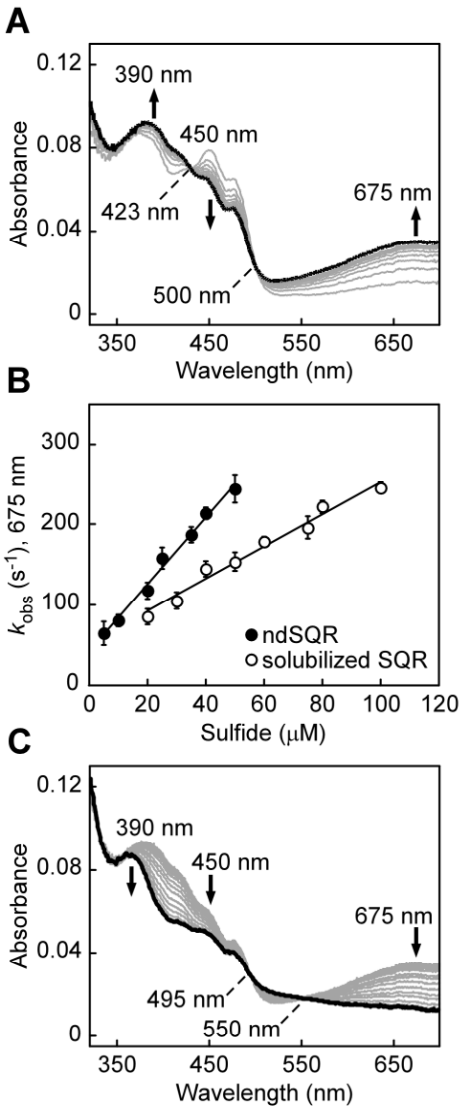

Figure 4. Rapid kinetics analysis of sulfide binding to *nd*SQR. *A*, *nd*SQR (20 μM) in 100 mM potassium phosphate buffer, pH 7.4, was rapidly mixed 1:1 (v/v) with Na_2S (40 μM) and monitored over a period of 3 s for CT complex formation (thick black line). *B*, Dependence of the k_{obs} for CT complex formation on the sulfide concentration for *nd*SQR (closed circles) versus detergent solubilized SQR (open circles). The data represent the mean ± standard deviation for three independent experiments. *C*, Decay of the *nd*SQR charge transfer complex formed with 10 μM *nd*SQR and 20 μM Na_2S, which was monitored over a period of 70 s, and was accompanied by flavin reduction at 450 nm (thick black line).

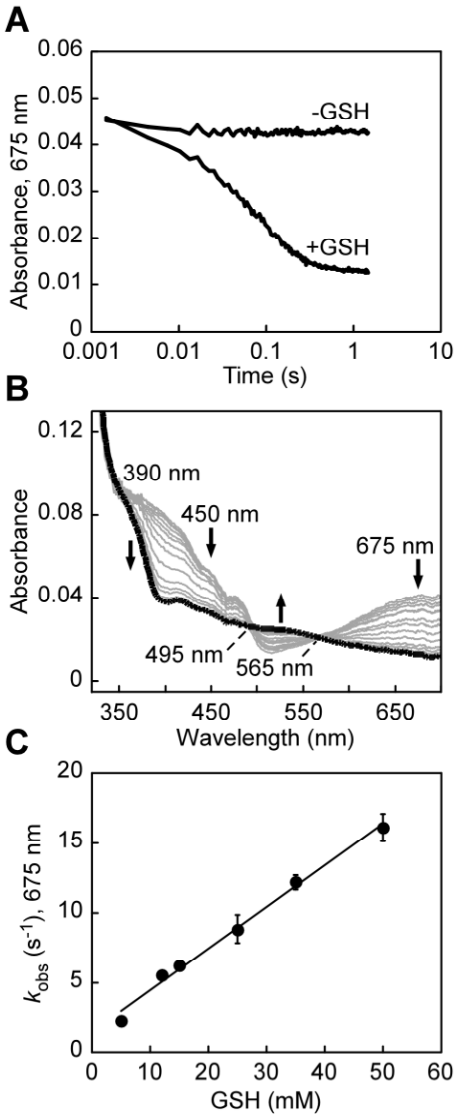

Figure 5. Disappearance of the sulfide-induced CT complex of *nd*SQR in the presence of GSH. *A, nd*SQR (40 μM) in 100 mM potassium phosphate buffer, pH 7.4, was rapidly mixed 1:1 (v/v) with Na_2S (80 μM) and aged for ~35 ms to form the CT complex, after which the mixture was rapidly mixed 1:1 (v/v) with 100 mM potassium phosphate buffer, pH 7.4 ± GSH (50 mM). The absorbance at 675 nm was monitored over a period of 3 s. *B,* Spectral changes accompanying the disappearance of the CT complex in the presence of 25 mM GSH, monitored over 3 s, which demonstrated reduction of FAD (thick black line). *C,* Dependence of the k_{obs} for the disappearance of the CT complex in *nd*SQR on the GSH concentration. The data represent the mean ± standard deviation for two independent experiments.

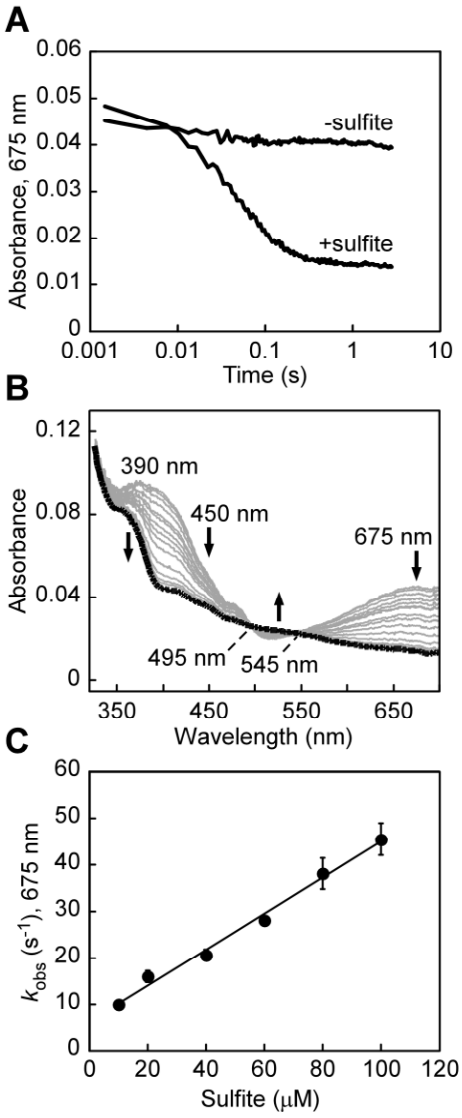

Figure 6. Disappearance of the sulfide-induced CT complex in *nd*SQR in the presence of sulfite. *A, nd*SQR (40 μM) in 100 mM potassium phosphate buffer, pH 7.4, was rapidly mixed 1:1 (v/v) with Na_2S (80 μM) and aged for ~35 ms to form the CT complex, after which the mixture was rapidly mixed 1:1 (v/v) with 100 mM potassium phosphate buffer, pH 7.4 ± sulfite (40 μM). The absorbance at 675 nm was monitored over a period of 3 s. *B,* Spectral changes accompanying the disappearance of the CT complex in the presence of 20 μM sulfite, monitored over 3 s, which demonstrated reduction of FAD (thick black line). *C,* Dependence of the k_{obs} for the disappearance of the CT complex in *nd*SQR on the sulfite concentration. The data represent the mean ± standard deviation for two independent experiments.

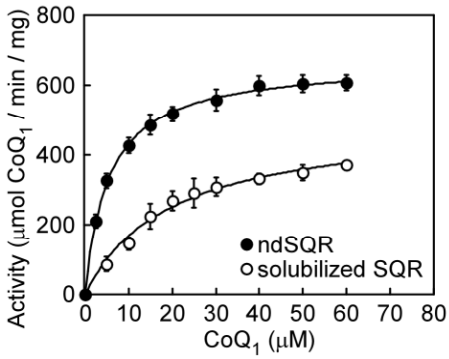

Figure 7. Kinetic analysis of *nd*SQR-mediated quinone reduction. The dependence of the activity of *nd*SQR (closed circles) and detergent solubilized SQR (open circles) on CoQ_1 concentration. The reactions included 0.8 mM sulfite as the acceptor in 100 mM potassium phosphate buffer, pH 7.4 containing 0.06 mg mL^{-1} BSA, 1 nM SQR, and 150 μM sulfide at 25 °C. Assays with solubilized SQR were conducted in the presence of 0.03% DHPC. The data represent the mean ± standard deviation for three independent experiments in which each CoQ_1 concentration was assayed in duplicate.

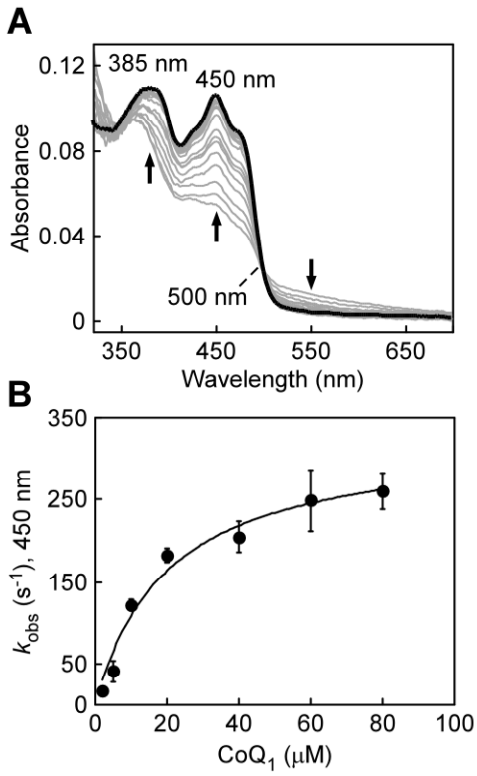

Figure 8. Kinetics of FAD oxidation in *nd*SQR by coenzyme Q_1. *A, nd*SQR containing reduced FAD (20 μM) was produced via photoreduction as described under Experimental Procedures, followed by reaction by 1:1 (v/v) rapid mixing with CoQ_1 (40 μM) for 5 s, which resulted in the oxidation of FAD (thick black line). *B*, Dependence of the k_{obs} for *nd*SQR-mediated CoQ_1 reduction on the concentration of CoQ_1. The data represent the mean ± standard deviation for two independent experiments.

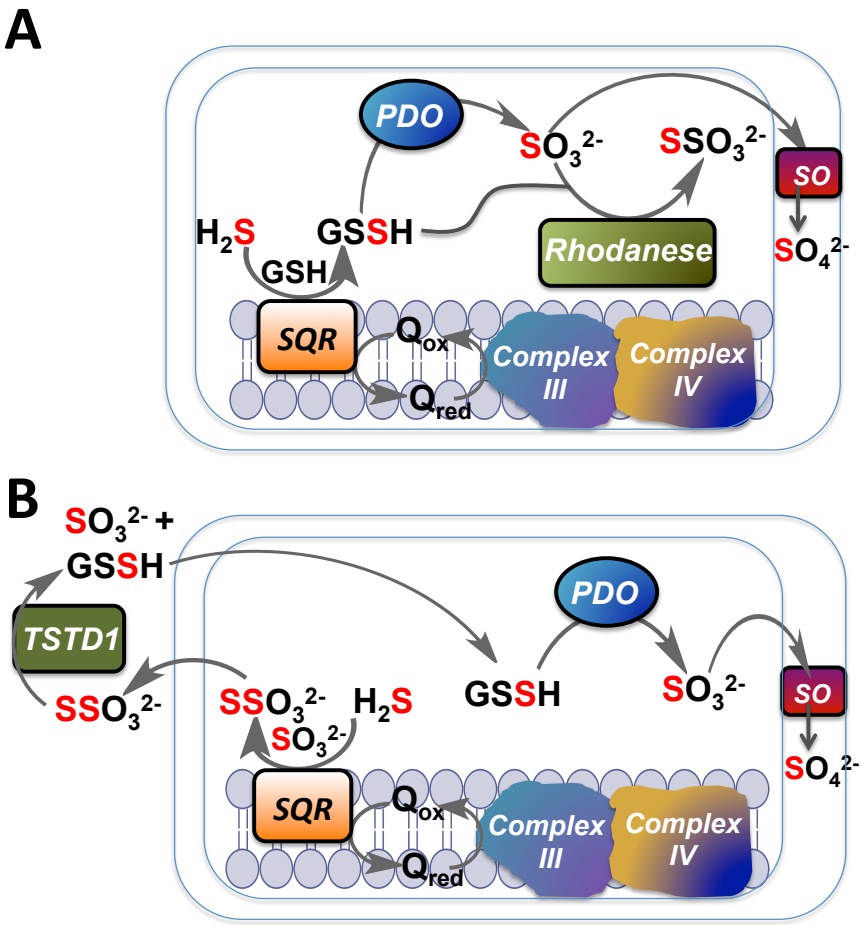

Figure 9. Implications of GSH versus sulfite as sulfane sulfur acceptor from SQR on the organization of the mitochondrial sulfide oxidation pathway. *A,* Transfer of 2-electron oxidized sulfide to GSH forms GSSH, which is converted by PDO to sulfite. The latter is a substrate for sulfite oxidase (SO), which resides in the intermitochondrial membrane space and is further oxidized to sulfate. In this scheme, rhodanese forms thiosulfate from GSSH and sulfite generated in the mitochondrion. *B*, Transfer of 2-electron oxidized sulfide from SQR to six-electron oxidized sulfite, generates thiosulfate, which must be transported out of the mitochondrion to undergo a second sulfur transfer reaction catalyzed by TSTD1. The product GSSH, which is highly reactive, must be transported back into the mitochondrion for utilization by PDO. The sulfur atoms derived from H_2S are shown in red. The metabolic logic of pathway B was described as "convoluted" even by its proponents (11) and for reasons discussed in the text, is considered to be unlikely.

H_2S oxidation by nanodisc-embedded human sulfide quinone oxidoreductase

Aaron P Landry, David P Ballou and Ruma Banerjee

J. Biol. Chem. published online May 16, 2017
